Heated fiber-optic cables for distributed dry density measurements of granulated bentonite mixtures: Feasibility experiments

Toshihiro Sakaki [a,b,*], Berrak Firat Lüthi [a], Tobias Vogt [a], Masao Uyama [c], Sumio Niunoya [c]

[a] National Cooperative for the Disposal of Radioactive Waste (Nagra), Wettingen, Switzerland
[b] Department of Civil and Earth Resources Engineering, Kyoto University, Japan
[c] Nuclear Waste Technology Department, Obayashi Corporation, Tokyo, Japan

HIGHLIGHTS

- Laboratory experiments with fiber-optic cable emplaced in granulated bentonite with various known dry densities.
- Fiber-optic cable was electrically heated and temperature changes were measured by fiber-optic cable.
- Temperature changes highly reflected differences in dry density.
- Heated fiber-optic showed high potential as a quality control tool.

ARTICLE INFO

ABSTRACT

In the Swiss concept for the disposal of spent fuel and vitrified high-level radioactive waste, the buffer material of the engineered barrier system in the disposal tunnels consists of granulated bentonite mixtures (GBM) and blocks of highly compacted bentonite. For the GBM to perform sufficiently as a barrier, the dry density of the emplaced GBM is an essential parameter as well as a quality control indicator at the time of tunnel backfilling. In this study, an actively heated fiber-optic cable combined with distributed temperature sensing was applied with the aim of estimating the in-situ dry density distribution of the GBM. A set of experiments was performed using GBM specimens with controlled dry density conditions at the Grimsel Test Site in Switzerland to examine how the thermal responses vary with the dry density of the GBM material. The results indicated that the thermal responses were sufficiently sensitive to allow distributed temperature sensing in combination with an actively heated fiber-optic cable to be used as a reliable tool for estimating the dry density profile in the tunnels backfilled and sealed with the GBM along the cable with a high resolution.

1. Introduction

Distributed temperature sensing (DTS) is a technology for measuring temperature along a fiber-optic (FO) cable, which acts as a distributed temperature sensor. DTS yields a continuous temperature profile along the FO cable over a length up to several kilometers with a spatial resolution from decimeter to meter and sampling time of seconds to hours. The DTS and other distributed FO sensing technologies have been developed in the recent years. Nowadays, the DTS technology is widely used in various industrial applications focusing often on fire and leakage detection of assets and infrastructure objects as well as dam and levee monitoring.[1] In addition, in recent years DTS found its way in several hydrological studies (e.g.[2]) and geotechnical/geohydrological applications as summarized in Ref. [3].

In most DTS applications, the temperature profile is measured in a passive manner. More recently, active heating of a FO cable combined with DTS technology was successfully used for investigating soil moisture (e.g.[4–8]) water leakage in an embankment (e.g.[9]), or hydraulic conductivity in aquifers (e.g.[10]). Throughout this paper, in order to distinguish between the newer method and conventional passive temperature monitoring, the method that involves heating of FO cables is referred to as "active DTS".

Active DTS involves electrical heating of the FO cable and measuring temperature responses along the cable, which are strongly affected by the thermal properties of the material surrounding the FO cable. Heat transfer from a line source is well understood and described, e.g. Ref. [11], and has recently been studied in bentonite in Ref. [12]. This principle is used for the classic single-needle heat

* Corresponding author at: Department of Civil and Earth Resources Engineering, Kyoto University, Japan.
E-mail address: sakaki.toshihiro.2m@kyoto-u.ac.jp (T. Sakaki).

pulse probe (e.g.[13]), which has a typical needle length of 0.03–0.10 m (e.g.[14]) and is used to determine the thermal properties, e.g. of soils. The single-needle heat pulse probe measurement is thus considered rather as a "point" measurement at the location where the needle is emplaced. In the active DTS method, on the other hand, a several hundred meter to kilometer long heatable fiber-optic cable is used as the line heat source. The advantage of the active DTS over the needle heat pulse probe is that it enables the estimation of thermal property distribution along a long profile in the order of several kilometers with a typical spatial resolution of 0.25–2.0 m as determined by the DTS unit's capability.

Thermal conductivity is the main parameter controlling the heat transfer when the heat pulse method is used in unsaturated porous media. The thermal conductivity of unsaturated soils varies with porosity, or equivalently dry density, and water content (e.g.[15–21]). To estimate soil water content, the dependence of the soil's thermal properties on water content was used in several active DTS studies[4–6,22]. Likewise, the dependence of the thermal properties on the dry density implies that the active DTS can be used for estimating the dry density.

Dry density is an important parameter for many engineering problems involving buffer material in the engineered barrier system, which is a typical feature in concepts for deep geological disposal of radioactive waste.[23] The buffer forms the barrier between the disposal tunnel surface and the waste canister. Its main objectives in the Swiss disposal concept are to ensure low diffusive solute transport rates, to retard the transport of radionuclides from the buffer, to ensure migration of gas without compromising the hydraulic barrier, to reduce microbial activity, to mechanically buffer the canister and keep it in a stable position, and to allow dissipation of the heat generated by the waste to the rock mass so that the temperature of the canister, buffer and the rock are kept at maximum favorable conditions.[24] In the Swiss concept for the disposal of spent fuel/vitrified high-level waste, the buffer consists of granulated bentonite mixtures (GBM) and blocks of highly compacted bentonite.[23] Bentonite is essentially a natural clay mixture consisting mostly of montmorillonite of volcanic and hydrothermally altered origin. The waste canisters are first emplaced on the bentonite blocks inside the disposal tunnel, and the void space between the canisters and the tunnel wall is backfilled with GBM using screw feeders.[25]

As noted earlier, the dry density of the emplaced GBM controls the thermal, hydraulic and mechanical properties of the buffer of the engineered barrier system such as the thermal conductivity and hydraulic conductivity (e.g.,[26,27]). Thus, during backfilling of the repository tunnel with GBM to create the buffer, the target dry density is set and the dry density of the emplaced GBM is the key parameter for the initial quality control at the time of emplacement. As the saturation of the buffer in a clay host rock is a slow process due to small inflow rates from the rock into the tunnels, in-situ dry density can be measured shortly after the emplacement of the GBM with a known water content.

The dry density of the emplaced GBM is usually determined by mass and volume measurements for small-scale laboratory experiments and real-scale applications.[25] With this technique, potential local density variations cannot be evaluated within the measured volume. Only a very limited number of methods are available for investigation of spatial dry density variations, e.g. geophysical logging tools (e.g. gamma–gamma density log), dielectric tools[28,29] and heat pulse sensors[25]. However, these methods are more suited for mock-up tests for which detailed installation of the sensors is possible. Moreover, long dielectric profile sensors used in the mock-up tests in Ref. 28 and 29 are limited up to 1 m and typical heat pulse sensors provide only point measurements[25]. Therefore, their coverage depends directly on the number of sensors. On the other hand, a single FO cable with a small diameter can cover a large distance up to kilometers and provide a measurement profile with dm–m spatial resolution. It also has to be noted that the disturbance caused by a FO cable is minimal compared to that by conventional sensors where a bunch of many cables must be routed, which could induce significant disturbances to the GBM.

To demonstrate the feasibility of the active DTS method as a tool for estimating in-situ dry density distribution of GBM along a FO cable, a set of fundamental experiments were performed under well-controlled conditions at the Grimsel Test Site (GTS) in Switzerland. This paper reports the experimental tasks and results; (1) to examine how the thermal responses from the active DTS tests vary with the dry density of the GBM material, (2) to obtain a relationship between the thermal conductivity measured by the active DTS and dry density of GBM, and (3) to examine the feasibility of active DTS as a tool to measure dry density of GBM.

2. Material and methods

2.1. Temperature measurement with DTS

The DTS unit, to which the FO cable is connected, hosts a laser generator as well as a detector with a signal processing unit. The DTS unit in this study determines backscatter location via an optical time domain reflectometer[30] and uses the Raman backscatter characteristics of light emitted following a laser pulse into the FO cable. The Raman backscatter consists of two components of different wavelengths, the Stokes color characterized by a larger wavelength than that of the original pulse and anti-Stokes color with a smaller wavelength. A measurement of their ratio in time allows calculation of the temperature along the FO cable as a function of distance.[31,32] Compared to other FO sensing techniques, e.g. fiber bragg gratings as well as Brillouin and Rayleigh-based distributed systems, the most prominent advantage of the Raman-based DTS is that it is sensitive solely to temperature and not to strain. Modern DTS units have relatively high temperature measurement accuracies in the range of 0.001–0.5 °C depending on sampling time (the longer the sampling time, the better the accuracy).

2.2. Granulated bentonite mixture (GBM)

The GBM material used in this study is referred to as mixture 2.[33] It was made by compressing raw sodium bentonite material mined in Wyoming, USA, to a pellet dry density of 2180 kg/m^3 and crushing the pellets with an industrial blender to have a grain size distribution similar to the Fuller curve[33,34] with a maximum grain diameter of 6 mm shown in Fig. 1. The initial water content was 5.5% by weight. The water content was chosen such to have a raw material close to Proctor's optimum, to obtain the highest possible pellet dry density. A combination of a high pellet density and adequate grain size distribution leads to an optimal mixture dry density when emplaced.

The thermal conductivity of the GBM material was characterized in separate tests. A small cell (0.06 m in diameter, 0.15 m in height) equipped with a 0.10 m long heat pulse needle probe (KD2 Pro thermal analyzer TR-1 probe, Decagon Devices, Inc.) was first filled with the GBM as loosely as possible. The GBM was compacted in steps to various dry densities. The compaction was done through gently and uniformly tapping the cell wall to obtain as homogeneous a compaction as possible. The heat pulse probe needle was placed vertically at the bottom of the cell pointing upwards so that the measured thermal conductivity was representing an averaged value even if there was a slight vertical heterogeneity in the compacted GBM. The thermal conductivity of the GBM material obtained under a wide range of dry density shown in Fig. 2 ranged from 0.256 W/mK (for the loosely packed) to 0.559 W/mK (for the tightly packed condition).
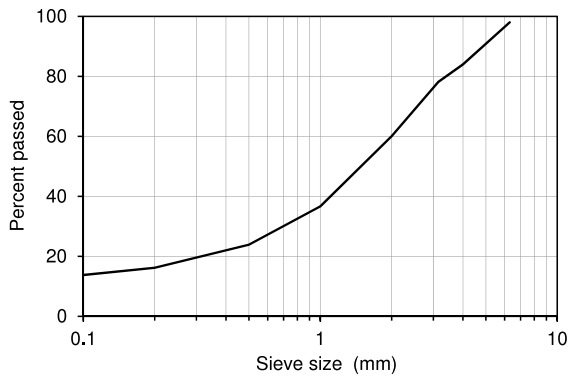
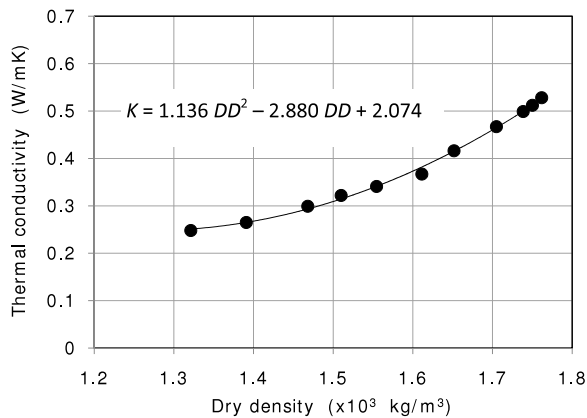**Fig. 1.** Grain size distribution of GBM mixture 2.[33]

Fig. 2. Thermal conductivity of GBM mixture 2 under varied dry density conditions separately measured by a thermal analyzer (with the TR-1 single needle sensor, 10 min read time and high power mode). The equation is the best-fit quadratic function. The water content was constant at 5.5% by weight.
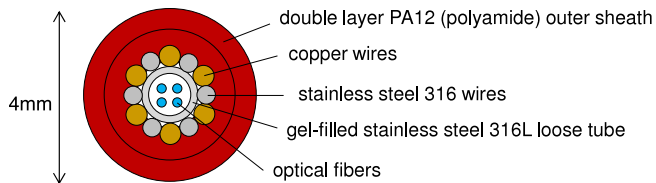

Fig. 3. Schematic cross-section of the heatable fiber-optic cable. Copper wires with a total cross-section of 0.83 mm².
Source: Figure adopted from Brugg Cable[38] and revised

2.3. Experimental setup

2.3.1. Heatable fiber-optic (FO) cable

The heatable fiber-optic (FO) cable used in this study was a multi-component cable (BRUsens LLK-BSTH 85 °C[38], Fig. 3) manufactured by Brugg Cable AG in Switzerland. The outer diameter was 4 mm. Four optical fibers (two single-mode, two multi-mode) were embedded loosely in the central gel-filled stainless steel tube surrounded by stainless steel and copper wires as well as polyamide sheaths for protection and strength. We used only one of the single-mode fibers for Raman spectra DTS. The length of the FO cable used in this study was 150 m.

Both ends of the 150 m-long FO cable were equipped with E2000 end connectors. The copper wires on both ends were extended with a copper cable for better wiring. The extended copper wire was selected to have a larger cross-section to reduce electrical resistance and thus to avoid an unnecessary temperature rise along the extended part.

2.3.2. Raman DTS unit

The Raman DTS unit used in this study was the Ultima S (Silixa Ltd, UK) with the finest spatial resolution of 0.25 m (defined as the length over which 10%–90% of a step temperature change can be detected) along the FO cable over the maximum length of 5000 m[40]. The sampling resolution (defined as the intervals in length at which temperature values are reported), d*x*, can be set either to 0.127, 0.254, 0.508 or 1.017 m.

Two PT100 temperature sensors can be hooked up to the DTS unit for calibration and/or measurement of reference temperatures. The DTS unit was calibrated using an ice bath with a temperature of 0 °C. Due to the stable tunnel climate conditions at the GTS, the calibration could be done in a stable environment. Furthermore, no temporal drift was observed due to the constant temperature inside the DTS unit. The accuracy of the measured temperature was calculated as the root mean square error, $RMSE = \frac{1}{n}\sqrt{\sum_1^n (T_{DTS} - T_{REF})^2}$ where, T_{DTS} and T_{REF} are the temperatures measured by DTS and PT100 in the reference ice bath, respectively, which was found to be 0.003 °C when the DTS measurement was done with a 0.127 m sampling resolution and 30 s sampling time. All the DTS measurements were performed with the single-ended configuration where only one end of the fiber-optic was connected to the DTS unit.

2.3.3. Power supply unit for heating

A current generator (hereafter the power supply unit) was used to induce heat along the FO cable. A power supply unit Delta Elektronika Model SM 52 AR 60 (max current 15.6 A, max voltage 53.1 V) was selected[39]. This unit can generate a power up to ~5.5 W/m with the 150 m-long cable.

2.3.4. Experimental setup for the heating tests

For the active DTS heating tests, the items described above were assembled to a configuration shown in Fig. 4. Eight boxes (0.128 m in inner width x 0.122 m in inner height x 1 m in length) were used to make two separate 4 m-long sections. These were core boxes made of plywood used to store borehole core samples. In order to assess the dimensions of the core boxes, a set of three-dimensional finite element heat transfer simulations were performed prior to the assembly of the apparatus. The results indicated that the heat (with 2 W/m heating power) from the FO cable would propagate through the bentonite and reach the boundary walls roughly after one hour. Therefore, the above-mentioned cross-sectional dimensions of the boxes were estimated to be sufficiently large so that the temperature data are free of effects from the walls at least up to one hour after the heating has started. Four boxes (boxes 1–4) were placed one after the other on a flat concrete slab. The other four boxes (boxes 5–8) were placed parallel to boxes 1–4.

The FO cable was placed in the slit on the endplates (Fig. 4). Between the endplates (i.e. inside each box), the FO cable was fixed along the centerline with a thin twist tie wire at every 0.25 m. Between boxes 1–4 and 5–8, exactly 2 m of the FO cable was left in the ambient air.

One of the 4 m sections was tightly filled with the GBM to the mean dry density of 1790 kg/m³. A rubber mallet and a wooden piece were used to compact the GBM as tightly and uniformly as possible.[35] The other 4 m section was, on the other hand, to have a low thermal conductivity, loosely filled with the GBM to a mean dry density of 1350 kg/m³. In these boxes, the GBM was poured as gently as possible to achieve the lowest dry density.

One end of the FO cable was connected to the DTS unit for single-ended temperature measurements. The copper wires at both ends of the FO cable were connected to the power supply unit
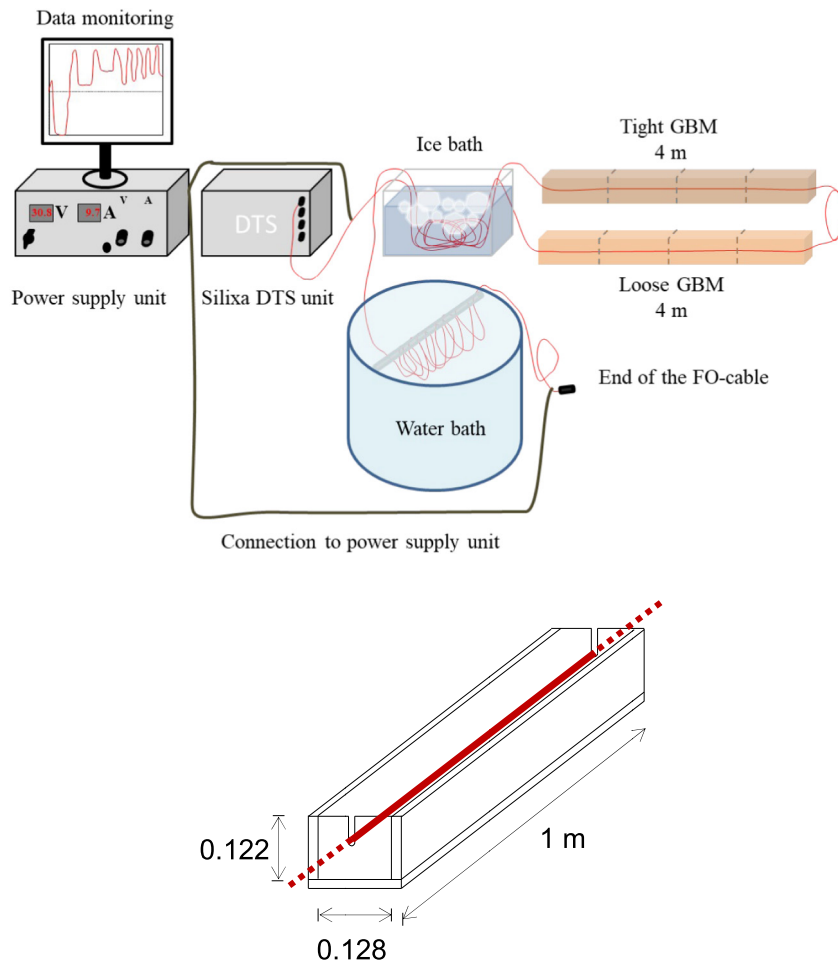
Fig. 4. Schematic image of the experimental setup. (Top) Entire setup with ice water and water baths, (bottom) detailed image of one of the boxes, lid not shown.

for heat generation. Some meters of the FO cable before the boxes with GBM were placed in ice water to perform and check the DTS temperature calibration as mentioned earlier. The rest of the FO cable after the GBM boxes was submerged in a large barrel filled with water with ambient temperature to prevent overheating of this cable section. Without having this part placed in water, the temperature of this section rose at a faster rate and reached the maximum temperature limit for the cable used due to the low thermal conductivity of air and having the rolled FO cables close to each other. Two PT100 temperature sensors were connected to the DTS unit, one placed in the ice water for calibration, the other placed in air for recording ambient air temperature.

2.3.5. Determination of setting parameters

The DTS unit offers several options for setting parameters, including sampling resolution (i.e. interval in length) and sampling time. For tests using the active DTS, heating power and duration are also essential parameters. A series of preliminary tests were performed with the goal of identifying the setting parameters that are well suited for estimating the dry density of the GBM. In these tests, two extreme conditions (i.e. lowest and highest dry densities) were considered.

Sampling time. The sampling time dt is the time interval over which the optical data are to be collected and averaged. A longer sampling time reduces the measurement error which is proportional to $1/\sqrt{dt}$.[36] With dt = 5, 10, 20, 30, and 60 s, increasing the dt from 5 to 30 s reduces the error roughly by a factor of 3. A

further increase of dt from 30 to 60 s does not lead to a significant improvement. Thus, dt = 30 s was selected. The measurement accuracy with the selected sampling time was calculated approximately as 0.003 °C with RMSE method.

Sampling resolution. The ULTIMA-S offers four sampling resolutions of 0.127, 0.254, 0.508, and 1.017 m. The FO cable is virtually divided into subsections having the length specified by the sampling resolution. In this study, the finest sampling resolution was selected so that temperature data were reported every 0.127 m along the FO cable. Note here that the "spatial resolution" is a distance over which 90% of a step temperature change can be detected. For Ultima S unit, the spatial resolution is 0.25 m when the sampling resolution is set to 0.127 m[40].

Heating power. Based on the finite element scoping calculations with varied power of 1–5 W/m, a heating power of 2 W/m was selected with an expected temperature rise of 3.2 °C in the tight GBM and 5.4 °C in the loose GBM. The temperature rise was found to be sufficiently high to get a clear heating signal, but also small enough to prevent unnecessary moisture movement.

Heating duration. Although the majority of the temperature changes takes place within the first 15–30 min, the heating duration was set to t_h = 3 h in order to obtain sufficient d$T(t)$ data during the heating phase. Heating with a power of 2 W/m was performed for 3 h followed by overnight cooling.

2.3.6. Test cases

The temperature response was examined for four dry density conditions. As noted above, the first 4 m section (boxes 1–4) was filled to a mean dry density of 1790 kg/m^3. This was the maximum dry density achievable by manual compaction. The boxes with the maximum dry density remained unchanged during the course of all tests.

The dry density of the GBM in the second 4 m section, which was first packed as loosely as possible, was increased in steps from 1350 (test 1) to 1500 (test 2) and 1650 (test 3) kg/m^3 (Fig. 5, Table 1). The density was increased by carefully tapping the walls and top surface with a rubber mallet. As the GBM settles, a small amount of GBM was added to keep the volume constant. This was repeated until all the pre-determined mass of GBM was added in the boxes to reach the next dry density.

After the packing was completed, the surface of the GBM was covered with a plastic wrap to avoid moisture exchange with the air, a wooden lid was placed on top, and a sufficient time was allowed for the system to thermally equilibrate.

2.3.7. Thermal conductivity estimation based on temperature data

When the water content of the GBM remains constant, e.g. at the time of emplacement in a tunnel with small water inflows, the thermal conductivity and therewith the thermal response measured by the heated FO cable are solely dominated by its dry density. The heating of a long FO cable can be approximated by the heat transfer around an infinite line source which can be found elsewhere, e.g., Ref. 11. The temperature changes (dT) when plotted against ln t exhibits a linear behavior. The thermal conductivity K is then estimated by the following equation:

$$K = Q/4\pi a \tag{1}$$

where, Q is the applied power in W/m, a is the slope of the d$T-\ln t$ data. As the very early data do not follow the linearity, they are typically excluded from the fitting process (e.g.[14]).

With a constant water content, the obtained K is a function of the dry density as seen in Fig. 2. Once the relationship between the estimates of K yielded by the active DTS and dry density is known, the dry density profile of the GBM can be determined from the K distribution along the FO cable.

3. Experimental results and discussion

3.1. Temperature changes during the heating tests

The obtained temperature changes in the three heating tests are plotted in Fig. 6. The results in test 1 showed that, the mean temperature changes (red and blue lines) were distinctly different in the tight and loose GBMs. The variation across four tight GBM boxes (1–4, light blue lines) and loose boxes (5–8, light red lines) was small. Under the loosest and tightest conditions, gentle pouring and hard compaction are believed to have yielded homogeneous dry density within the boxes (thus, around the FO cable).

In test 2 where the GBM in boxes 5–8 were slightly compacted, the mean temperature in these boxes still showed more increase than that in boxes 1–4 but less than those in test 1. This was expected as the compaction progresses, the dry density and therewith thermal conductivity increases leading to a less temperature increase. It has to be noted that, in the medium loose boxes, the variation within boxes 5–8 was somewhat pronounced. It was suspected that tapping the box walls to increase the dry density might have led to a less homogeneous density in some boxes. Although the mean dry density of each box was controlled, the local density around the FO cable could have been somewhat different.

Test 3, where the dry density of the GBM in boxes 5–8 was further increased, resulted in a mean temperature rise even less than that in test 2. The d$T(t)$ curves in boxes 5–8 were quite similar and showed only a small variation. Controlling the GBM dry density around the FO cable to a known condition was found to be essential for acquisition of an accurate temperature response under various density conditions. This suggests that, for achieving a homogeneous compaction for intermediate dry densities, the packing method has to be refined.

3.2. Estimation of thermal conductivity

Towards the goal of estimating the dry density of the GBM from the thermal responses, the thermal conductivity was calculated using the collected d$T(t)$ data. For the four different dry densities examined in heating tests 1–3, the mean dT curves were plotted against ln t and a linear function was fitted as in Fig. 7. The data for the first 3 min (ln $t = 5.19$, shaded) did not follow a linear behavior and were excluded from the fitting. Data after one hour (ln $t = 8.18$, shaded) were also excluded from the fitting due to the possible effects from the box wall boundaries. The effects are seen as a slight increase in the slope resulting from a lower thermal conductivity of the wooden walls and air outside. The slope of the fitted linear functions was used to calculate the thermal conductivity using Eq. (1). The obtained results are summarized in Table 2.

The active DTS-estimated thermal conductivity values were then plotted against those estimated by the thermal analyzer in Fig. 8. In general, a good agreement was observed between the two. For the medium loose boxes (1500 kg/m^3), the active DTS-estimated thermal conductivity was slightly higher than the thermal analyzer results. As noted above, compaction of the GBM was done by tapping the box walls and adding the predetermined amount of the GBM. In this study, the compaction method had not been standardized and the heterogeneity was not checked. Although packing was done with care, we suspect that slight density variations within the test boxes might have affected the temperature response along the FO cable.

For the highest dry density (1790 kg/m^3), the active DTS-estimated thermal conductivity was slightly lower than the results of the thermal analyzer. The FO cable consists of multiple elements as shown in Fig. 3. The optical fibers in the middle are surrounded by the heating elements, which are then protected by the outer sheath material (Polyamid Nylon PA12, thermal conductivity = 0.25–0.35 W/mK, Brugg Cables, Switzerland). The thermal conductivity of the outer sheath is lower than that of the GBM when highly compacted. The temperature responses measured by the fiber optic for the highest density with a thermal conductivity of 0.559 W/mK can also reflect the thermal property of the outer sheath material with a lower thermal conductivity. Although further study is needed, this could have contributed to the slight underestimation.

3.3. Calibration to dry density

In Fig. 9, the dry density (average of boxes 1–4 = 1790 kg/m^3, average of boxes 5–8 = 1350, 1500, and 1650 kg/m^3) is plotted against the DTS-estimated thermal conductivity. For each box, five thermal conductivity values were calculated using the temperature data obtained at every 0.127 m in the central 0.508 m interval. Based on the scatter of the obtained thermal conductivities, the standard deviation was computed and 95% confidence intervals are also plotted. The narrow 95% confidence intervals indicate that the error is quite small.

A quadratic function was fitted to the mean of the active DTS-estimated thermal conductivities. For the range of the dry density
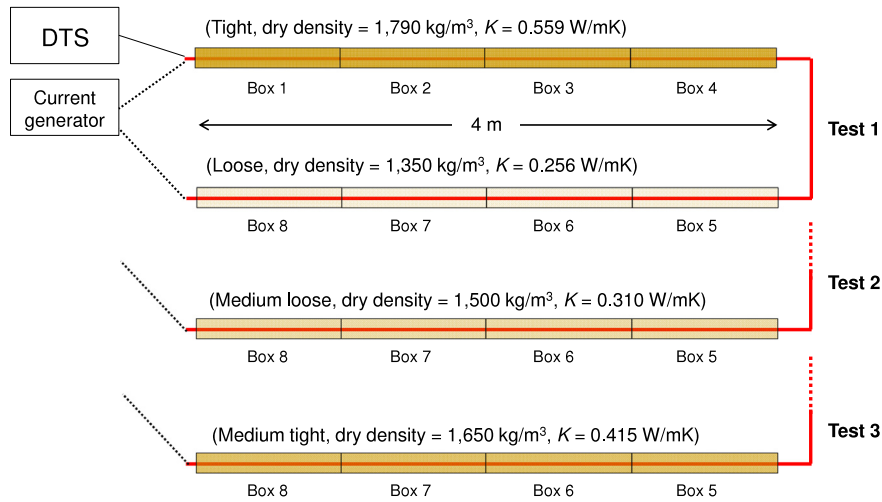
Fig. 5. Test setup with various density conditions. The dry density in boxes 1–4 remained unchanged whereas that in boxes 5–8 was increased in steps. The thermal conductivity values shown were those separately measured by thermal analyzer (Table 1).

Table 1
Conditions of GBM in each test.

Test no.	Boxes 1–4[*]			Boxes 5–8		
	Packing condition	Dry density (kg/m³)	Thermal conductivity[**] (W/mK)	Packing condition	Dry density (kg/m³)	Thermal conductivity[**] (W/mK)
1	Tight	1,790	0.559	Loose	1,350	0.256
2	Tight	1,790	0.559	Medium loose	1,500	0.310
3	Tight	1,790	0.559	Medium tight	1,650	0.415

[*] Remained unchanged during three tests.
[**] Separately measured by thermal analyzer (Fig. 2)
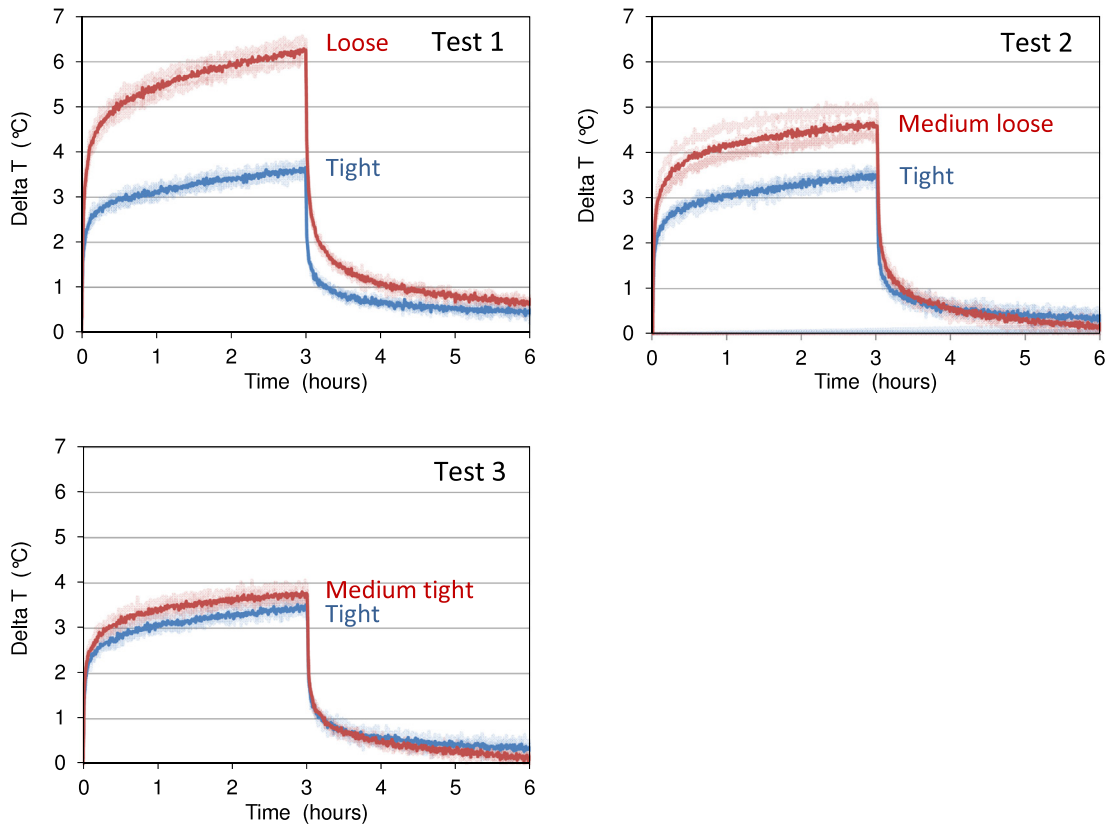
Fig. 6. Temperature changes for three test cases. Dark blue: average of boxes 1–4. Light blue: central 0.508 m average in each of boxes 1–4. Dark red: average of boxes 5–8. Light red: central 0.508 m average in each of boxes 5–8.

Table 2
Comparison of thermal conductivity values calculated from the slope with those measured separately using a thermal analyzer.
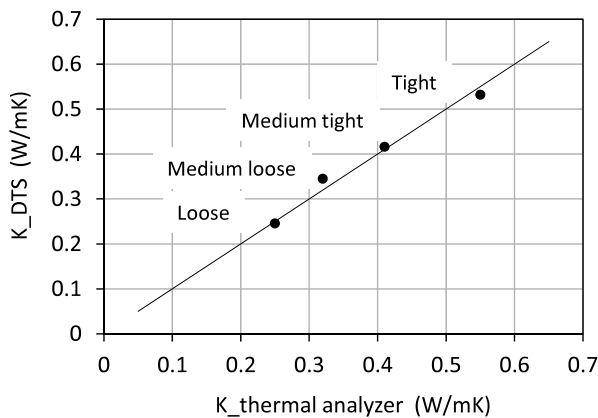
| GBM condition | Mean dry density (kg/m^3) | Thermal conductivity K (W/mK) | | Remark |
		Thermal analyzer[*]	DTS using Eq. (1)	
Loose	1,350	0.256	0.246 (0.007)[**]	Boxes 5–8 (test 1)
Medium loose	1,500	0.310	0.345 (0.020)[**]	Boxes 5–8 (test 2)
Medium tight	1,650	0.415	0.416 (0.021)[**]	Boxes 5–8 (test 3)
Tight	1,790	0.559	0.532 (0.020)[**]	Boxes 1–4 (tests 1–3)

[*] Measured using KD2 Pro, TR-1, high power mode, read time 10 min, values shown are estimated using the fitted equation in Fig. 2
[**] Values in the parentheses; standard deviation based on five thermal conductivity values computed for the central 0.508 m of each box
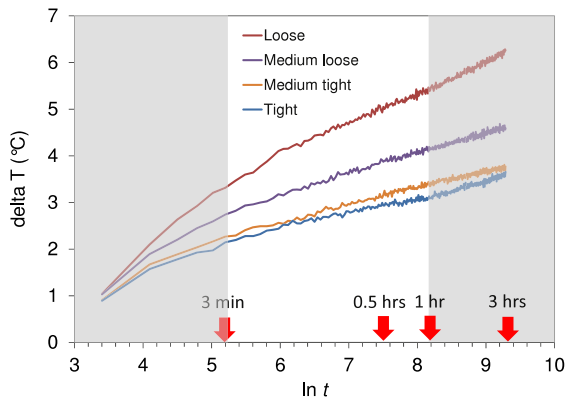
Fig. 7. Temperature rise in the heating phase plotted as a function of ln t (t in s). Shaded parts (0–3 min and 1–3 h) were excluded from the fitting of a linear function.
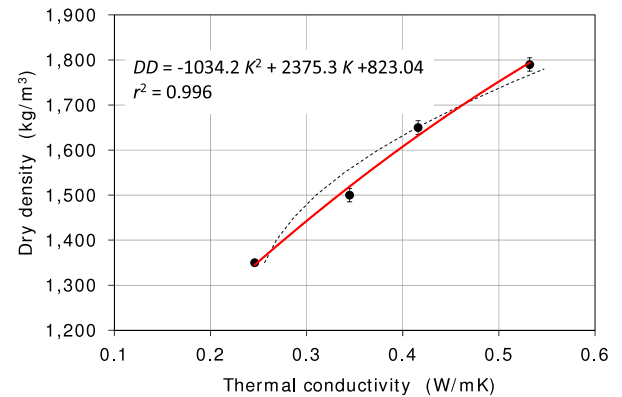

Fig. 9. Active DTS calibrated to dry density of GBM mixture 2 based on dT-ln$t$ data for 3–60 min under Q = 2 W/m. Circles: measured, Red line: fitted, Dashed line: relationship by thermal analyzer in Fig. 2.

Fig. 8. Comparison of thermal conductivity values estimated with active DTS and those determined with thermal analyzer. The line is a 1 : 1 line.

considered in this study, the r^2 value was 0.996 and the results clearly showed that the active DTS-estimated thermal conductivity can be converted into dry density. For comparison purposes, the dashed line is the relationship presented in Fig. 2. The slight difference between the dashed and the red curves results from the discrepancy described in Fig. 8.

4. Conclusions

The heat pulse needle probe is well established and a good choice for point measurement of thermal properties and dry density of GBM in relatively small scale (cm–dm) laboratory experiments. For large-scale applications (tens to hundreds of meters), however, the point sensors are not suited in the sense that a large number of sensors are needed to generate sufficient data to cover

a large distance or area. Due to their small diameter, long life-time and ability to provide temperature at high spatial resolution with high accuracies, heating of FO cables is considered highly suited for determining the distribution of the thermal properties and density along the FO cable.

A series of experiments was performed to demonstrate the feasibility of the active DTS for estimating the dry density of GBM along the FO cable. The dry density of the GBM considered in the experiments ranged over 1350–1790 kg/m^3, which corresponded to the thermal conductivity of 0.256–0.559 W/mK. For the active DTS tests, the following conditions were employed:

- Sampling resolution = 0.127 m
- Sampling time = 30 s
- Heating power = 2 W/m
- Heating duration = 3 h

A sampling time of 30 s seemed reasonable as smaller sampling times resulted in more noise, whereas increasing the sampling time did not lead to a significant improvement in reducing the noise of 30 s.

The heating power of 2 W/m induced a reasonable increase in temperature in the test GBM with a low water content of 5.5%. The resulting temperature changes were sufficient to be reliably detected and it was also assumed that they would not affect the moisture conditions around the FO cable during the heating duration. For materials with a higher thermal conductivity (e.g. higher water content), a higher power might be necessary to induce a reasonable temperature rise. Although not shown, heating with a varied heating power of 1–5 W/m for 60 min, the temperature rises in GBM with dry densities of 1350 and 1790 kg/m^3 ranged between 2.6–13.5 and 1.5–7.3 °C, respectively. Under the conditions tested in the experiments, the range of the heating power

of 1–5 W/m covered well the practical range that could induce reasonably detectable temperature changes (1 W/m seemed to be the low end). The temperature rise was roughly proportional to the heating power. The experimental results thus indicated that the active DTS-generated temperature data were sufficiently sensitive to the dry density of the GBM surrounding the FO cable. The active DTS-estimated thermal conductivity values were calibrated to the mean dry density of the GBM in the test boxes using a quadratic equation. The high r^2 value and narrow 95% confidence intervals indicated that the dry density could be estimated from the thermal conductivity.

The thermal conductivity values estimated using the $dT(t)$ of the active DTS data obtained for four different dry densities of the GBM differed slightly compared to those measured separately with the thermal analyzer. For the highest dry density condition, the DTS slightly underestimated the thermal conductivity. The plastic shield material of the FO cable, whose thermal conductivity was about half of the GBM's thermal conductivity when tightly compacted, could have contributed to the underestimation of the bulk thermal conductivity. This effect should be further quantified in future studies. In addition, the FO cable selection is crucial and has to consider not only mechanical protection but also appropriate thermal properties.

On the other hand, the active DTS-estimated thermal conductivity being higher than that measured with the thermal analyzer for the medium loose case has likely resulted from slight spatial density variations in the test boxes. Sample preparation in bentonite and clay-based materials is known to be challenging and to have an impact on several properties.[37] The compaction method used in this study seemed to have yielded reasonable mean dry densities, however, the packing method for more homogeneous sample preparation needs further improvement.

It was also found that the rolled portion of the FO cable that was exposed to air reached its maximum temperature limit. To avoid this issue, this section had to be placed in a large water bath. The heating can be further optimized by connecting the power unit to the FO cable just before and after the test interval.

Nonetheless, the calibration of active DTS-estimated thermal conductivity to the dry density of GBM showed high potential as a tool for estimating the dry density of GBM. The above findings could vary for different experimental conditions such as the heating power, GBM water content, and/or FO cable type (size, material, or structure). To ensure a high accuracy, similar calibration curves should be established for each active DTS test by taking the specific conditions into account. Once the curves have been developed, the temperature changes along the FO cable can be converted to the distribution of the thermal conductivity, from which dry density or water content profiles can be inferred.

Acknowledgments

References

1. Inaudi D, Cottone I, Figini A. Monitoring Dams and Levees with Distributed Fiber Optic Sensing, In: The 6th International Conference on Structural Health Monitoring of Intelligent Infrastructure 2013, December 9-11, Hong-Kong 2013.

2. Selker JS, Thevenaz L, Huwald H, et al. Distributed fiber-optic temperature sensing for hydrologic systems. Water Resour Res. 2006a;42W12202. http://dx.doi.org/10.1029/2006wr005326.

3. Schenato L. A review of distributed fibre optic sensors for geo-hydrological applications. Appl Sci. 2017;7(9):896. http://dx.doi.org/10.3390/app7090896.

4. Cao D, Shi H, Zhu G, Wei SE, Chen J, Yan B. A distributed measurement method for in-situ soil moisture content by using carbon-fiber heated cable. J Rock Mech Geotech Eng. 2015;7:700–707. http://dx.doi.org/10.1016/j.jrmge.2015.08.003.

5. Ciocca F, Lunati N, van de Giesenand I, Parlange MB. Heated optical fiber for distributed soil-moisture measurements: A lysimeter experiment. Vadose Zone J. 2012. http://dx.doi.org/10.2136/vzj2011.0199.

6. Sayde C, Gregory Ch, Gil-Rodriguez M, et al. Feasibility of soil moisture monitoring with heated fiber optics. Water Resour Res. 2010;46:W06201. http://dx.doi.org/10.1029/2009WR007846.

7. Weiss JD. Using fiber optics to detect moisture intrusion into a landfill cap consisting of a vegetative soil barrier. J Air Waste Manage Assoc. 2003;53:1130–1148. http://dx.doi.org/10.1080/10473289.2003.10466268.

8. Striegl AM , Loheide II SP. Heated distributed temperature sensing for field scale soil moisture monitoring. Ground Water. 2012;50:340–347. http://dx.doi.org/10.1111/j.1745-6584.2012.00928.x.

9. Perzlmaier S, Straer K.H., Strobl T., Aufleger M. Integral seepage monitoring on open channel embankment dams by the DFOT heat pulse method. In: Proceedings of the 74th Annual Meeting, Int. Comm. on Large Dams, Barcelona, Spain 2006.

10. Bense F, Read O, Bour T, et al. Distributed temperature sensing as a downhole tool in hydrogeology. Water Resour Res. 2016;52:9259–9273. http://dx.doi.org/10.1002/2016WR018869.

11. Carslaw HS, Jaeger JC. Conductivity on of Heat in Solids. 2nd ed., Oxford, UK: Clarendon Press; 1959.

12. Valter M, Puzrin AM, Plötze M. Discrete geometry model of heat in granular bentonite barriers. Environ Geotech. 2018;5(2):3–17. http://dx.doi.org/10.1680/jenge.15.00052.

13. Bristow KL, White GJ, Kluitenberg RD. Comparison of single and dual probes for measuring soil thermal properties with transient heating. Aust J Soil Res. 1994;32:447–464.

14. Decagon Devices, Inc . KD2 Pro Thermal Properties Analyzer Operator'S Manual. 2016:67.

15. Johansen O. Thermal Conductivity of Soils. [Ph.D diss], Trondheim.Norwegian Univ. of Science and Technol; 1975 (CRREL Draft Transl. 637, 1977).

16. Campbell GS, Jungbauer JD, Bidlake WR, Hungerford RD. Predicting the effect of temperature on soil thermal conductivity. Soil Sci. 1994;158(5):307–313.

17. Lu S, Ren Y, Gong T, R. Horton. An improved model for predicting soil thermal conductivity from water content at room temperature. Soil Sci Soc Am J. 2007;71(1):8–14. http://dx.doi.org/10.2136/sssaj2006.0041.

18. Smits KM, Limsuwat A, Sakaki T, Illangasekare TH. Thermal conductivity of sands under varying moisture and porosity in drainage-wetting cycles. Vadose Zone J. 2010;9(1):172–180. http://dx.doi.org/10.2136/vzj2009.0095.

19. Tarnawski VR, Momose T, Leong WH, Bovesecchi G, Coppa P. Thermal conductivity of standard sands. Part I. Dry-state conditions. Int J Thermophys. 2009;30:949. http://dx.doi.org/10.1007/s10765-009-0596-0.

20. Tarnawski VR, Momose T, Leong WH. Thermal conductivity of standard sands. II Saturated conditions. Int J Thermophys. 2011;32:984. http://dx.doi.org/10.1007/s10765-011-0975-1.

21. Tarnawski VR, McCombie ML, Momose T, Sakaguchi I, Leong WH. Thermal conductivity of standard sands. Part III. Full range of saturation. Int J Thermophys. 2013;34(6):1130–1147. http://dx.doi.org/10.1007/s10765-013-1455-6.

22. Sayde C, Buelga JB, Rodriguez-Sinobas L, et al. Mapping variability of soil water content and flux across 1–1'000 m scales using the actively heated fiber optic method. Water Resour Res. 2014;50:7302–7317. http://dx.doi.org/10.1002/2013WR014983.

23. Nagra . In: Project Opalinus Clay: Demonstration of Disposal Feasibility for Spent Fuel, Vitrified High-Level Waste and Long-Lived Intermediate-Level Waste - Safety Report (Entsorgungsnachweis) Nagra technical report, NTB 02-05. Wettingen, Switzerland: Nagra; 2002.

24. Nagra . In: Montmorillonite stability under near-field conditions, Nagra technical report, NTB 14-12. Wettingen, Switzerland: Nagra; 2014.

25. Müller HR, Garitte B, Vogt T, et al. Implementation of the full-scale emplacement (FE) experiment at the Mont Terri rock laboratory. Swiss J Geosci. 2017. http://dx.doi.org/10.1007/s00015-016-0251-2.

26. Villar MV, Lloret A. Influence of dry density and water content on the swelling of a compacted bentonite. Appl Clay Sci. 2008;39:38–49. http://dx.doi.org/10.1016/j.clay.2007.04.007.

27. Alonso EE, Alcoverro L, Malinsky V, et al. The febex benchmark test: Case definition and comparison of modelling approaches. Int J Rock Mech Min Sci. 2005;42:611–638. http://dx.doi.org/10.1016/j.ijrmms.2005.03.004.

28. Sakaki T, Köhler S, Müller HR. FE Experiment: Density measurement of granulated bentonite mixture in a 2D pre-test using a dielectric moisture profile probe, In: P-04-02, Clay Conference 2015, March 23-26, Brussels, Belgium 2015a.

29. Sakaki T, Köhler S, Hertrich M, Müller HR. FE Experiment: Density measurement of granulated bentonite mixture in a 3D 1:1 scale mockup test using dielectric tools, In: P-04-03, Clay Conference 2015, March 23-26, Brussels, Belgium. 2015b.

30. Dakin JP, Pratt GW, Bibby DJ, Ross JN. Distributed optical fibre raman temperature sensor using a semiconductor light source and detector. *Electron Lett*. 1985;21(13):569–570. http://dx.doi.org/10.1049/el:19850402.

31. Hausner MB, Suarez F, Glander KE, Giesen NVD, Selker JS, Tyler SW. Calibrating single-ended fiber-optic raman spectra distributed temperature sensing data. *Sensors*. 2011;11:10,859–10,879. http://dx.doi.org/10.3390/s111110859.

32. Tyler SW, Selker JS, Hausner MB, et al. Environmental temperature sensing using Raman spectra DTS fiber-optic methods. *Water Resour Res*. 2009;45(4):1–11. http://dx.doi.org/10.1029/2008WR007052.

33. Garitte B, Weber HP, Müller HR, et al. Requirements, manufacturing and QC of the buffer components Report, LUCOEX – WP2, 2015:115.

34. Fuller WB, Thomson SE. *The Laws of Proportioning Concrete*. New York. Transactions of the American Society of Civil Engineers LIX; 1907 Dec. 1907.

35. Sakaki T, Illangasekare TH. Comparison of height-averaged and point-measured capillary pressure - saturation relations for sands using a modified Tempe cell. *Water Resour Res*. 2007;43W12502. http://dx.doi.org/10.1029/2006WR005814.

36. Selker JS, van de Giesen N, Westhoff M, Luxemburg WMJ, Parlange MB. Fiber optics opens window on stream dynamics. *Geophys Res Lett*. 2006b;33L24401. http://dx.doi.org/10.1029/2006GL027979.

37. Matusewicz M, Pulkkanen V-M, Olin M. Influence of sample preparation on MX-80 bentonite microstructure. *Clay Miner*. 2016;51(2):189–195. http://dx.doi.org/10.1180/claymin.2015.051.2.06.

38. Brugg Cables. BRUsens Temperature 85 °C heatable, Fibre Optic Sensing Cable, 2015, 2012/10/16 Rev. 05 BK ©www.bruggcables.com/sensing.

39. Delta Elektronika. *DC Power Supplies*. Delta Elektronika.2015 http://www.delta-elektronika.nl/.

40. Silixa Ultima User Manual. 2015, Silixa Ltd 2015,www.silixa.com.